Plasma Sources Science and Technology

PAPER

Effect of the plasma-induced magnetic field on a magnetic nozzle

IOP Publishing

Plasma Sources Science and Technology

Plasma Sources Sci. Technol. **25** (2016) 045012 (9pp)

doi:10.1088/0963-0252/25/4/045012

Effect of the plasma-induced magnetic field on a magnetic nozzle

Mario Merino and Eduardo Ahedo

Equipo de Propulsión Espacial y Plasmas (EP2), Universidad Carlos III de Madrid, 28911 Leganés, Spain

E-mail: mario.merino@uc3m.es

Received 8 March 2016, revised 19 April 2016
Accepted for publication 10 May 2016
Published 21 June 2016

Abstract

A two-fluid, two-dimensional model of the plasma expansion in a divergent magnetic nozzle is used to investigate the effect of the plasma-induced magnetic field on the acceleration and divergence of the plasma jet self-consistently. The induced field is diamagnetic and opposes the applied one, increasing the divergence of the magnetic nozzle and weakening its strength. This has a direct impact on the propulsive performance of the device, the demagnetization and detachment of the plasma, and can lead to the appearance of zero-field points and separatrix surfaces downstream. In contrast, the azimuthal induced field, albeit non-zero, is small in all cases of practical interest.

Keywords: magnetic nozzle, plasma expansion, electric propulsion, plasma thruster

(Some figures may appear in colour only in the online journal)

1. Introduction

A magnetic nozzle (MN) is an axisymmetric, longitudinal magnetic field with a convergent-divergent (or merely divergent) geometry that can guide, expand and accelerate a plasma [1–6]. MNs are promising for space plasma propulsion thanks to their ability to contactlessly accelerate and control in-flight a high velocity plasma jet. As a consequence, several next-generation plasma thrusters under active development employ a MN as their main acceleration stage [7–15]. Once the plasma has been accelerated by the MN, it needs to detach itself from the magnetic lines to form a free plasma plume before these lines begin to turn around to close upon themselves (see [16–18] and references therein). Detachment is not a problem for other applications of MNs such as advanced manufacturing and material plasma processing [19, 20] or plasma wind tunnels [1], where the goal is just to direct the plasma jet against a material target in a controlled manner.

To obtain the desired 'nozzle' effect and guide the plasma along the magnetic lines requires that at least the electrons be well magnetized in the near region of the MN, where the plasma jet is being accelerated. This is ensured in current devices, which use magnetic fields in the order of a few hundreds of Gauss. The applied magnetic field strength is nonetheless insufficient to magnetize the heavier ions in the cases of interest, except perhaps near the throat region. In this regime, electrons follow the magnetic tubes, and ions expand and accelerate thanks to the ambipolar plasma electric field that ensues [6, 21]. Indeed, unmagnetized ions are desirable for the adequate plasma detachment in propulsive applications [18].

The electric currents that develop in the plasma induce a magnetic field whose relative intensity, with respect to the applied one, scales with the plasma β parameter. As the plasma density is increased, so does β, and at some point the plasma-induced field becomes a major feature of the expansion, which can modify the total field strength and thus deform the shape of the MN. The natural question that arises then is on the magnitude of these effects and their consequences on the operation of the MN, and in particular, on the generation of magnetic thrust and the downstream detachment of the plasma jet. Works by Arefiev and Breizman [22] and Winglee *et al* [23] reported a paramagnetic character of the plasma currents, so that the plasma-induced magnetic field reinforces the applied field and reduces the MN divergence. In these works, it is argued that this would circumvent the plasma detachment problem, since the plasma would actually carry the (frozen) magnetic lines within itself, 'ironing out' the MN down to infinity.

However these theories do not apply to a plasma thruster where the hot plasma created inside a plasma source is expanded supersonically in a divergent MN. Ahedo showed that in a column of magnetized plasma, azimuthal electron currents of a diamagnetic character are created from the radial balance between resistive and magnetic forces [24]. These currents induce a magnetic field that tends to cancel the applied one at the center of the source; for β of order unity, the plasma remains only marginally magnetized near the source walls [25]. This situation is also the one expected by Gerwin [26]. Then, Ahedo and Merino showed that the diamagnetic azimuthal electron currents are transported downstream into the near-collisionless MN keeping isorotation [6]. It was also shown that while partially-magnetized ions can develop a paramagnetic current in the MN region, it is marginal compared to the dominant diamagnetic electron current in all cases of practical interest [17]: only in the case of an initially-hypersonic plasma entering the MN (i.e. cold) or extreme ion magnetization levels can the plasma exhibit a net paramagnetic character.

Beyond that direct evidence of the diamagnetism of the plasma in a MN, it is worth highlighting that this is inherent to the radial confinement and supersonic axial expansion of a hot plasma jet and to the generation of positive magnetic thrust, which have been confirmed experimentally [27]. Indeed, in the case of Arefiev and Breizman, the plasma is quasi-cold, and the paramagnetic currents induce a deceleration (magnetic drag) on the plasma beam.

The major goal of this work is to present a consistent 2D theory on the influence of the plasma-induced magnetic field on the expansion of a hot, non-uniform plasma jet in a MN and similar magnetic configurations. Although both azimuthal and longitudinal induced fields will be discussed, the focus is placed in the longitudinal field, which is stronger and the one directly involved in magnetic thrust generation and the deformation of the magnetic nozzle geometry. The theory will confirm that, in a propulsive MN, the induced magnetic field (i) opposes the externally-applied field (ii) opens the magnetic tubes of the MN, *increasing* its divergence, and (iii) *weakens* the magnetic strength of the MN, promoting the earlier demagnetization (and detachment) of the plasma.

The rest of this paper is structured as follows. Section 2 presents the 2D plasma/MN model with induced magnetic field. Section 3 discusses the longitudinal induced magnetic field in a simplified 1D paraxial geometry to identify its key effects on the MN. Section 4 integrates the full 2D model using an iterative scheme for the solution of the self-consistent longitudinal and azimuthal induced field and conducts the parametric investigation of the expansion. Lastly, section 5 highlights the main conclusions of this work.

2. Plasma expansion model

The two-fluid plasma/MN model introduced in [6] is extended here to include the plasma-induced magnetic field. The model describes the axisymmetric, collisionless, quasineutral expansion of a supersonic plasma composed of hot, fully-magnetized, isotropic, Maxwellian electrons and cold, single-charged ions in a divergent magnetic field. Extensions of the model to include non-Maxwellian electrons [28] and warm ions [29] were studied elsewhere. Those effects do not change qualitatively the conclusions herein, and therefore are not treated below.

For the sake of illustration, the applied field of the MN is that of a single current loop of radius R_L located in the plane $z = 0$. The plasma flows inside this magnetic field toward $z > 0$. We will denote the applied, plasma-induced, and total magnetic field as $\boldsymbol{B}_a$, $\boldsymbol{B}_p$, and $\boldsymbol{B} = \boldsymbol{B}_a + \boldsymbol{B}_p$ respectively. A subindex '0' indicates values at the origin ($z = r = 0$): e.g. $B_{a0} = B_{az}(0, 0)$. We choose $B_{a0} > 0$ without loss of generality. As in [6], a tilde will be used to indicate the longitudinal component of a vector field: e.g. $\tilde{\boldsymbol{B}} = B_z\boldsymbol{1}_z + B_r\boldsymbol{1}_r = \boldsymbol{B} - B_\theta\boldsymbol{1}_\theta$, and the right-handed magnetic reference frame is introduced: $\{\boldsymbol{1}_\parallel, \boldsymbol{1}_\perp, \boldsymbol{1}_\theta\}$, with $\boldsymbol{1}_\parallel = \tilde{\boldsymbol{B}}/\tilde{B}$ and $\boldsymbol{1}_\perp = \boldsymbol{1}_\theta \times \boldsymbol{1}_\parallel$. Since the magnetic field is solenoidal, there exists a streamfunction ψ for its longitudinal components: e.g. $\partial\psi/\partial r = rB_z$ and $\partial\psi/\partial z = -rB_r$. In the same manner we define ψ_a for the applied field and ψ_p for the induced one, so that $\psi = \psi_a + \psi_p$. By convention, we shall take $\psi_a = \psi_p = \psi = 0$ at the axis.

Electrons are modeled as an isotropic Maxwellian species with an effective polytropic cooling law, $p_e \propto n^\gamma$ (where $p_e = nT_e$ is the electron pressure, $\gamma \geqslant 1$ is the polytropic cooling exponent, n the (quasineutral) plasma density, and T_e is the electron temperature). The value of γ that best approximates the behavior of the electron species seems to depend on the experimental setup, and ranges from near-isothermal values [4, 30] (< 1.1 to 1.3) to near-adiabatic values [31] (5/3). Recent kinetic models [32, 33] suggest a variable γ that is close to unity in the near region and increases downstream to describe the collisionless electron cooling. Under the assumption that $m_e u_e^2 \ll T_e$ (i.e. negligible electron inertia with respect to thermal motion) and $\ell_e \ll L$ (i.e. electron Larmor radius ℓ_e small compared to the macroscopic scale length, L), electron streamtubes coincide with magnetic streamtubes [6]. Observe, however, that electrons now follow the *total* magnetic field $\boldsymbol{B}$ instead of merely the applied one. Keeping only the non-zero components of the magnetic force on electrons, these equations read:

$$n\tilde{u}_e/B = G_e(\psi); \quad \tilde{\boldsymbol{u}}_e = u_{\parallel e}\boldsymbol{1}_\parallel \quad (\text{i.e.}: u_{\perp e} = 0), \tag{1}$$

$$0 = -\gamma T_e \nabla \ln\frac{n}{n_0} + e\nabla\phi - e(u_{\theta e}\tilde{B} - u_{\parallel e}B_{\theta p})\boldsymbol{1}_\perp, \tag{2}$$

where $G_e(\psi)$ is the electron flux-to-magnetic strength ratio on each streamtube, $\boldsymbol{u}_e$ the electron velocity, e the electron charge, and ϕ the ambipolar electric potential. The projection of the last equation along $\boldsymbol{1}_\parallel$ can still be integrated into:

$$H_e(\psi) = \begin{cases} \gamma(T_e - T_{e0})/(\gamma - 1) - e\phi & \text{if} \quad \gamma > 1, \\ T_{e0}\ln(n/n_0) - e\phi & \text{if} \quad \gamma = 1, \end{cases} \tag{3}$$

with $H_e(\psi)$ the Bernoulli function on each streamtube. Finally, the projection of equation (2) along $\boldsymbol{1}_\perp$ reads:

$$eu_{\theta e}\tilde{B} - eu_{\parallel e}B_{\theta p} = -\frac{\partial H_e}{\partial \boldsymbol{1}_\perp} \equiv -r\tilde{B}\frac{dH_e}{d\psi}, \tag{4}$$

from where it is easy to infer the diamagnetic character of the electron azimuthal current. As a side note, observe that the isorotation condition of the electron flow [34, 35] (i.e. $u_{\theta e}/r = \text{const.}$ along magnetic tubes) is only satisfied for $B_{\theta p}/\tilde{B} \to 0$, and that a positive $B_{\theta p}$ tends to increase $u_{\theta e}/r$.

The steady-state motion of ions is given by their continuity and momentum equations,

$$\nabla \cdot (n\boldsymbol{u}_\mathrm{i}) = 0, \tag{5}$$

$$m_\mathrm{i}(\boldsymbol{u}_\mathrm{i} \cdot \nabla)\boldsymbol{u}_\mathrm{i} = -e\nabla\phi + e\boldsymbol{u}_\mathrm{i} \times \boldsymbol{B} \tag{6}$$

where m_i and $\boldsymbol{u}_\mathrm{i}$ are respectively the ion mass and the ion velocity. By projecting equation (6) along $\boldsymbol{u}_\mathrm{i}$ and $\boldsymbol{1}_\theta$ one obtains

$$m_\mathrm{i}\frac{u_\mathrm{i}^2}{2} + e\phi = H_\mathrm{i}(\psi_\mathrm{i}), \tag{7}$$

$$r m_\mathrm{i} u_{\theta\mathrm{i}} + e\psi = D_\mathrm{i}(\psi_\mathrm{i}), \tag{8}$$

where ψ_i is the ion streamfunction that labels each ion streamtube and $H_\mathrm{i}(\psi_\mathrm{i})$, $D_\mathrm{i}(\psi_\mathrm{i})$ are the ion mechanical energy and the canonical angular momentum on each ion streamtube. The radius of the plasma, i.e. that of the plasma-vacuum interface, is denoted as $R_\mathrm{V}(z)$. At the throat section ($z = 0$) the plasma has a radius $R_0 < R_\mathrm{L}$ and is sonic. This is expressed by the ion Mach number at the origin, $M_0 = \tilde{u}_{\mathrm{i}0}/c_{\mathrm{s}0} = 1$, with $c_{\mathrm{s}0} = \sqrt{\gamma T_{\mathrm{e}0}/m_\mathrm{i}}$ the ion sonic velocity.

Finally, Ampère's law $\nabla \times \boldsymbol{B}_\mathrm{p} = \mu_0 \boldsymbol{j}$ relates the induced magnetic field to the electric currents in the plasma, $\boldsymbol{j} = en(\boldsymbol{u}_\mathrm{i} - \boldsymbol{u}_\mathrm{e})$. Written in terms of ψ_p and $B_{\theta\mathrm{p}}$, this equation becomes:

$$\frac{1}{r}\frac{\partial^2\psi_\mathrm{p}}{\partial z^2} + \frac{\partial}{\partial r}\left(\frac{1}{r}\frac{\partial\psi_\mathrm{p}}{\partial r}\right) = -\mu_0 j_\theta, \tag{9}$$

$$\frac{1}{r}\frac{\partial}{\partial r}(rB_{\theta\mathrm{p}}) = \mu_0 j_z; \quad \frac{\partial B_{\theta\mathrm{p}}}{\partial z} = -\mu_0 j_r, \tag{10}$$

with $B_{\theta\mathrm{p}}(z, 0) = 0$. Equations (9) and (10) show that the longitudinal induced field $\tilde{\boldsymbol{B}}_\mathrm{p}$ is caused only by the azimuthal plasma current j_θ, while the azimuthal induced field $B_{\theta\mathrm{p}}$ is caused by the longitudinal plasma current (and can be calculated from j_z alone).

The plasma momentum equation (i.e. the sum of equations (2) and (6)),

$$m_\mathrm{i}(\boldsymbol{u}_\mathrm{i} \cdot \nabla)\boldsymbol{u}_\mathrm{i} = -\gamma T_\mathrm{e}\nabla \ln\frac{n}{n_0} + \frac{\boldsymbol{j}}{n} \times \boldsymbol{B}, \tag{11}$$

shows that radial equilibrium at the throat requires a net diamagnetic plasma current $j_\theta \sim nT_\mathrm{e}/(R_0 B)$. Introducing this into Ampère's equation (9) it can be seen that

$$\frac{\tilde{B}_\mathrm{p}}{B_\mathrm{a}} \sim \mu_0\frac{nT_\mathrm{e}}{B_\mathrm{a}^2} = \beta_\mathrm{a}, \tag{12}$$

where β_a is the well-known thermal beta parameter based on the applied field, which is a measurement of the capability of the plasma to generate an induced magnetic field of sufficient strength to disturb the MN. Note that a factor 2 is sometimes included in this definition, but it is purposely omitted here.

Normalization of the model shows that the plasma expansion depends on: (i) the ratio R_0/R_L, which controls the divergence rate of the outermost magnetic line with plasma and the position of the turning point of the applied field (i.e. the location where this line turns around); (ii) the radial plasma profile at the throat; (iii) the 'effective electron cooling rate,' measured by γ; (iv) the ion dimensionless gyrofrequency at the origin, $\hat{\Omega}_{\mathrm{i}0} = eB_{\mathrm{a}0}R_0/\sqrt{m_\mathrm{i}T_{\mathrm{e}0}}$, which controls the applied field magnetic strength; and (v) the *plasma beta parameter at the origin*, defined as $\beta_{\mathrm{a}0} = \mu_0 n_0 T_{\mathrm{e}0}/B_{\mathrm{a}0}^2$. The first four dependencies have already been discussed in previous works [6, 29]; the fifth parameter is the fundamental one in the present discussion.

3. Paraxial 1D plasma expansion

The order of magnitude estimation in equation (12) already reveals the main dependencies of the induced magnetic field. Before carrying out the full 2D integration of the model, we can gain some physical insight into the problem by solving the analytical, paraxial expansion limit, that is, when the characteristic axial gradient length is $L_z \gg R_0$. This requires a slender and slowly-varying applied magnetic field, so that $u_{r\mathrm{i}} \ll u_{z\mathrm{i}}$ and $\boldsymbol{1}_\perp \simeq \boldsymbol{1}_r$. In practice, this is only true for a limited length and for $R_\mathrm{L}/R_0 \gg 1$.

For simplicity, we will assume that the radial plasma density profile is uniform and treat the expansion as 1D in first approximation. We shall further assume that ions do not have an initial rotation, so that, according to equation (8), $u_{\theta\mathrm{i}} \simeq 0$ everywhere in the paraxial limit. In this case, $j_\theta = 0$ except at the plasma edge $R_\mathrm{V}(z)$, where the electron diamagnetic drift current concentrates in a thin sheet of thickness $\mathcal{O}(\ell_\mathrm{e}) \ll R_0$ as shown in [6].

The ion equations of the model become simple algebraic relations:

$$nu_{z\mathrm{i}}/B = G_\mathrm{i}, \tag{13}$$

$$\frac{1}{2}m_\mathrm{i}u_{z\mathrm{i}}^2 + e\phi = H_\mathrm{i}, \tag{14}$$

where G_i, the ion-to-magnetic flux ratio, and H_i, the ion mechanical energy, are two upstream constants. Combining the last equation with equation (3) allows to eliminate ϕ. Note that H_e and H_i are now constant for all streamtubes. Neglecting radial ion inertia, the radial plasma momentum equation (equation (11) projected along $\boldsymbol{1}_r$) can be integrated into

$$nT_\mathrm{e} = \int_{R_V^-(z)}^{R_V^+(z)} j_\theta(r)B(r)\mathrm{d}r, \tag{15}$$

where the integration takes place across the current-sheet layer at the plasma border, $R_V(z)$. Since the paraxial limit of Ampère's equation states that

$$\frac{\mathrm{d}B}{\mathrm{d}r} = -\mu_0 j_\theta, \tag{16}$$

we can write this expression as

$$2\mu_0 nT_\mathrm{e} = B_\mathrm{ext}^2 - B_\mathrm{int}^2, \tag{17}$$

where B_ext and B_int are the strength of the magnetic field immediately outside and inside of the plasma tube, i.e. across the current-sheet layer.

This last equation shows that a discontinuity in the magnetic field exist across the current sheet in the macroscopic scale, which depends only on the local electron pressure at each section. This result can be interpreted as follows: the diamagnetic current induces a field B_p that opposes the applied one, reducing the magnetic strength inside the plasma, and in doing so, expelling a fraction of the magnetic flux out of it.

To close the paraxial model analytically, we need to consider the following additional approximation: the azimuthal current sheet in the plasma forms a very long tube whose radius and intensity varies only slowly, according to $L_z \gg R_0$. As such, to first order, the magnetic field it induces is restricted to the inside of the tube, just like an infinite solenoid. Under this assumption we can identify $B_{ext} = B_a$, the applied field, and $B_{int} = B = B_a + B_p$, the total magnetic field in the plasma. Then,

$$B^2/B_a^2 = 1 - 2\beta_a, \tag{18}$$

where again $\beta_a = \mu_0 n T_e / B_a^2$ is the *local* beta parameter based on B_a. A higher β_a clearly means a stronger induced field and therefore a lower total field, i.e. a weaker MN. Since β_a depends on the local electron pressure, the determination of B is coupled with the integration of the plasma expansion.

Naturally, two questions arise: first, whether β_a increases downstream so that B_p gains importance with respect to B_a, and second, whether the presence of induced field effects means a faster-diverging MN all the way to infinity. Rearranging equation (18) and using the definition of β_a,

$$\frac{1}{\beta_a} = 2 + \frac{B^2}{\mu_0 n T_e} = 2 + \frac{n_0^\gamma}{\mu_0 n_0 T_{e0}} \frac{B^2}{n^\gamma}. \tag{19}$$

Hence, β_a increases if n^γ decreases slower than B^2. The ordering of n can be easily obtained from equation (13), noting that far downstream,

$$u_{zi} \to \sqrt{\frac{\gamma T_{e0}}{m_i} \frac{\gamma + 1}{\gamma - 1}}, \tag{20}$$

i.e. a finite value when $\gamma \neq 1$. Hence, $n \propto B$ in the far expansion region. This means that β_a increases downstream for $\gamma < 2$, and therefore so does the induced magnetic field with respect to the applied one (note that in the isothermal case, $u_{zi} \sim \sqrt{-2(T_{e0}/m_i)\ln(n/n_0)}$ downstream instead, but the conclusion is still the same.). Clearly, a higher value of γ, i.e. a faster electron cooling, diminishes the relevance of the induced field in the far expansion region.

To answer the second question, observe that the evolution of $R_V(z)$ is given by $R_V(z)/R_0 = \sqrt{B_0/B(z)}$. Note, however, that in this model the value of B_0 depends on β_{a0} (i.e. the induced field can lower the value of B_0); moreover, the position of the MN throat itself may not coincide with the throat of the applied field. Nonetheless, comparing R_V against the case $\beta_{a0} = 0$, for which $R_V(z) = R_V(z)|_{\beta_{a0}=0}$, it can be seen that

$$\frac{R_V^4|_{\beta_{a0}=0}}{R_V^4} \propto \frac{B^2}{B_a^2}. \tag{21}$$

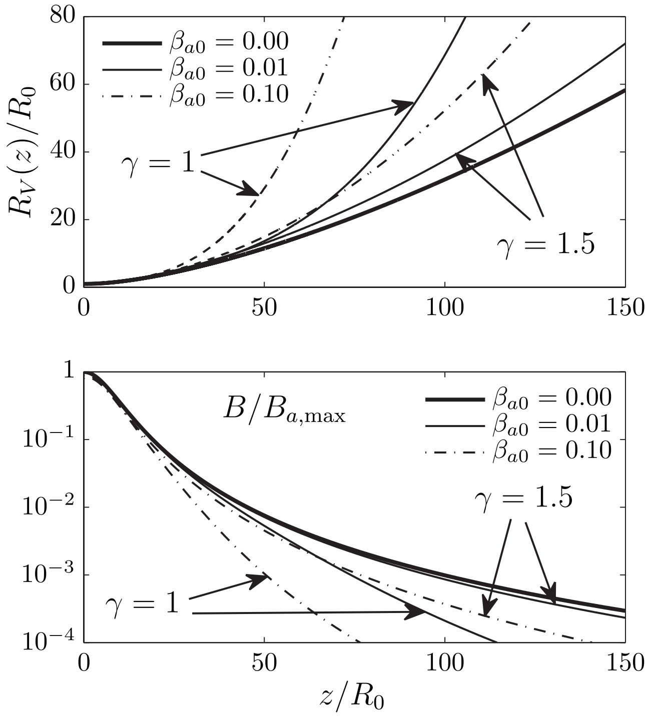

Figure 1. Plasma tube radius $R_V(z)$ and total magnetic field inside the plasma B in the paraxial limit, for $\beta_{a0} = 0$ (thick lines), $\beta_{a0} = 0.01$ (thin solid lines) and $\beta_{a0} = 0.1$ (dash–dot lines), and for $\gamma = 1$ and 1.5. For the purposes of presenting the results on a physical axial coordinate only, the axial magnetic field of a single current loop with $R_L = 10R_0$ has been used.

Hence, using equation (18) and since β_a increases downstream for $\gamma < 2$, so does $R_V/R_V|_{\beta_{a0}=0}$, and therefore the presence of an induced magnetic field results in a more divergent MN as $z \to \infty$.

The resulting model is completely algebraic and depends only on the parameters β_{a0} and γ. Figure 1 shows the shape of the resulting 1D MN and $B(z)$ for several values of these parameters, illustrating the weakening and opening of the MN downstream. As it can be observed, the effect of the induced field is maximal for an isothermal plasma, and increases with β_{a0}. A small displacement of the actual magnetic throat toward the downstream side takes place, which is insignificant for $\beta_{a0} \sim 0.1$ (and not noticeable in figure 1). All these phenomena can be regarded as the consequence of the diamagnetic nature of the plasma, which pushes against the applied magnetic field lines in the radial direction until a balance between the thermal pressure, nT_e, and the magnetic pressure, $B^2/(2\mu_0)$, is established.

While it provides valid trends in the low- and mild-β_a range, the quasi-1D model of this section suffers several limitations. First and foremost, the paraxial assumption is not a valid one in actual devices, where 2D effects can play an important role in the expansion, and there is a prominent turning-point for all magnetic lines except the central one; obviously, the turning point is missed in this approximation. Second, by keeping only the radial derivative in equation (16) this assumption has disregarded the elliptic character of equation (9) and considered only the local plasma currents for the determination of B_p; instead, in a 2D case the plasma currents at one point affect the magnetic field everywhere. Third, by dropping the radial ion inertia from equation (6) we have neglected the only paramagnetic current contribution in our model, i.e. the $j_{\theta\mathrm{i}}$ that develops downstream. Nonetheless, as shown elsewhere [18, 29], the magnitude of this paramagnetic current is upper-bounded, and moreover, in the parametric range of practical interest for propulsive applications, it is always small ($j_{\theta\mathrm{i}} \ll j_{\theta\mathrm{e}}$). As a side comment, it is worth pointing out that radial ion inertia is central in the radial balance between the magnetic and electric forces on ions, which determine the divergence of the ion streamlines and plasma detachment downstream. Without it, the computed ambipolar electric field is inconsistent in 2D models and the problem of detachment cannot be correctly analyzed [36]. Fourth, since the paraxial model does not allow the calculation of ion separation from the magnetic lines, it cannot recover the local *longitudinal* electric currents that develop in the plasma, and therefore cannot calculate $B_{\theta\mathrm{p}}$. All of these drawbacks, and the desire to study the radial variation of B_p, serve as the motivation to approach the analysis of the induced magnetic field effects with the full 2D treatment of the next section.

4. 2D integration and discussion

The DIMAGNO code [6], which uses the method of characteristics (MoC) to integrate the hyperbolic supersonic ion equations of the plasma expansion in the MN, has been extended to solve for the plasma-induced magnetic field $\boldsymbol{B}_\mathrm{p}$ and include the additional magnetic force terms in the ion and electron equation due to B_θ. Due to the elliptic character of equation (9), simultaneous integration of both the plasma and induced field would require abandoning the advantageous MoC approach. Instead, a convenient iterative procedure is used: an initial $\boldsymbol{B}_\mathrm{p}$ is assumed (e.g. $\boldsymbol{B}_\mathrm{p} = 0$), and a first plasma solution is obtained. The resulting plasma currents $\boldsymbol{j}$ are then used to refine the first estimate of $\boldsymbol{B}_\mathrm{p}$: the plasma domain is discretized into small cells, and the current of each cell is represented by an infinitesimal current loop. The integral solution of Ampère's equation (equation (9)) for such a loop is then used to compute each cell contribution to $\boldsymbol{B}_\mathrm{p}$ in an efficient manner. Feeding the induced magnetic field back into the MN model, the process is repeated until a convergence in $\boldsymbol{B}_\mathrm{p}$ and the plasma variables is achieved [37].

The numeric integration of the MN plasma flow and $\boldsymbol{B}_\mathrm{p}$ is carried out in the region between the throat and the downstream section $z = z_F$. Clearly, the plasma currents that exist upstream and downstream of this region can still affect what occurs within it, although, the magnetic influence of these currents decays cubically with distance. To compensate for the influence of downstream currents, the simulation results presented in this section refer only to roughly half of the integrated region, i.e. for $z < z_F/2$, and it has been checked that the plasma expansion and the magnetic field in the presented region are almost insensitive to the extension of the integration domain. On the other hand, the influence of the plasma currents upstream of the MN throat, which depend on the type of plasma source used, is neglected, on the basis that the applied field is strong in this region and the induced field effects there are small in the $\beta_{\mathrm{a}0}$ range under study.

To simplify the discussion in the rest of this section, only the isothermal case is considered ($\gamma = 1$). The following plasma profile is assumed at the MN throat for $r < R_0$,

$$n(0, r) = n_0 \exp(-3(r^2/R_0^2)\ \ln 10), \tag{22}$$

$$u_{z\mathrm{i}}(0, r) = u_{z\mathrm{e}}(0, r) = M_0\sqrt{T_{\mathrm{e}0}/m_\mathrm{i}}, \tag{23}$$

$$u_{r\mathrm{i}}(0, r) = u_{r\mathrm{e}}(0, r) = u_{\theta\mathrm{i}}(0, r) = 0, \tag{24}$$

$$\phi(0, r) = 0, \tag{25}$$

and it is injected into a MN with $R_\mathrm{L} = 3.5R_0$ and $\hat{\Omega}_{\mathrm{i}0} = 1$. To guarantee hyperbolicity in the whole plasma domain for the MoC we enforce $M_0 = 1.01$. Equation (4) at the throat is used to determine the profile of $u_{\theta\mathrm{e}}$,

$$u_{\theta\mathrm{e}} = -\frac{6T_{\mathrm{e}0}\ln 10}{e\tilde{B}}\frac{r}{R_0^2} \tag{26}$$

(observe that $B_{\theta\mathrm{p}} = 0$ at the throat since we have chosen $j_z = 0$ at $z = 0$).

We begin the discussion with the longitudinal induced magnetic field, $\tilde{\boldsymbol{B}}_\mathrm{p}$. The applied field $\boldsymbol{B}_\mathrm{a}$, the self-consistent $\tilde{\boldsymbol{B}}_\mathrm{p}$, the plasma current j_θ, and the local plasma beta for the case $\beta_{\mathrm{a}0} = 0.01$ are depicted in figure 2.

The marked 2D character of the azimuthal plasma currents and the induced magnetic field stands out in these graphs. Both are larger in a region around the axis, while the periphery of the plasma is almost unaffected, especially downstream. Interestingly, while j_θ decreases gradually as n drops downstream, $\tilde{B}_\mathrm{p}$ does not decrease as much and maintains its strength; moreover, the region around the axis where $\tilde{B}_\mathrm{p}$ is important grows radially. This agrees with the non-local nature of the induced field, which is generated not only by the local plasma currents but also by those upstream and downstream. It is easy to infer from these plots that the local value of $\tilde{B}_\mathrm{p}/B_\mathrm{a}$, i.e. the relative importance of induced field effects, increases fast downstream around the axis, in agreement with the 1D results, but only moderately so at the plasma edge. This behavior agrees well with the recovered 2D variation of the local β_a parameter in the last plot of figure 2, confirming its usefulness as an estimator of $\tilde{B}_\mathrm{p}/B_\mathrm{a}$, even if the actual value of $\tilde{B}_\mathrm{p}$ results from the resolution of the elliptic Ampère's equation (9).

The total longitudinal magnetic field is presented in figure 3 for $\beta_{\mathrm{a}0} = 0.01$, 0.05, and 0.1. Two related phenomena take place and become more pronounced as $\beta_{\mathrm{a}0}$ increases, namely: (i) the increase of MN divergence caused by $\tilde{\boldsymbol{B}}_\mathrm{p}$, and (ii) the reduction of the magnetic strength downstream. Once again, this is congruent with the net diamagnetic character of the plasma in a propulsive MN and the generation of positive thrust, and agrees with the results of the 1D model of section 3.

Interestingly, if $\tilde{B}_\mathrm{p}$ is large enough (i.e. for large enough values of $\beta_{\mathrm{a}0}$), the total magnetic field can eventually cancel out downstream. This can be already observed for $\beta_{\mathrm{a}0} = 0.05$

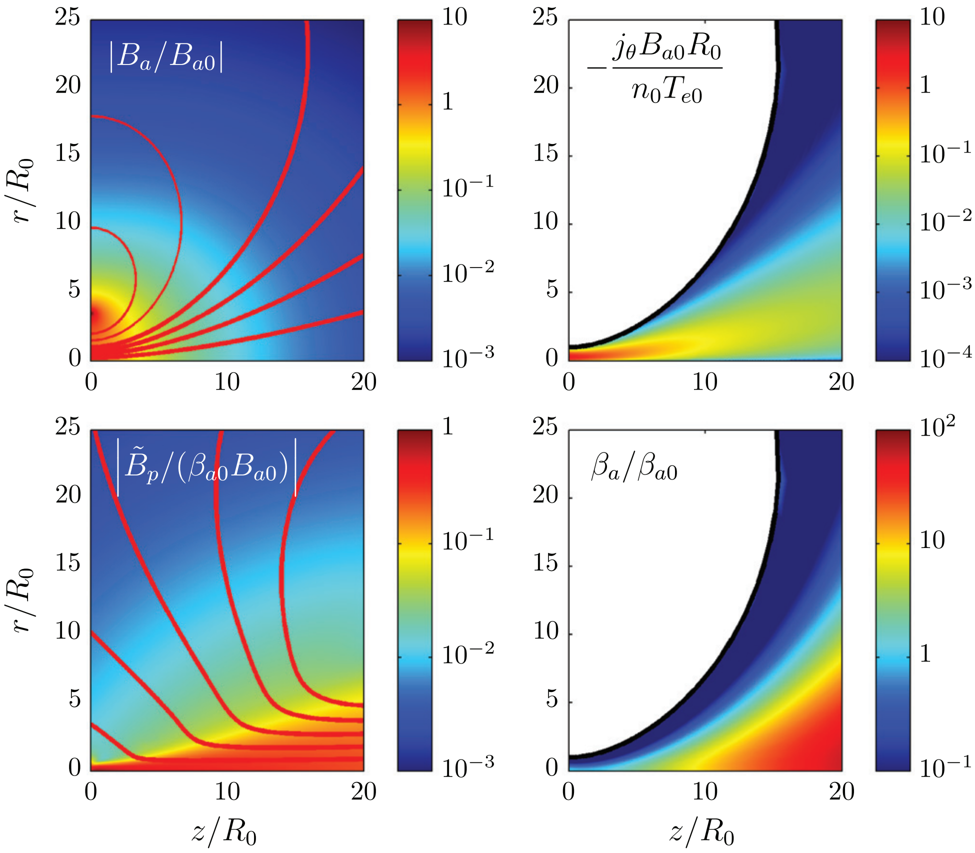

Figure 2. Applied field $\boldsymbol{B}_{\mathrm{a}}$, induced field $\tilde{\boldsymbol{B}}_{\mathrm{p}}$, azimuthal plasma current j_θ and local plasma beta β_{a} in the $\beta_{\mathrm{a0}} = 0.01$ case ($\gamma = 1$, $R_{\mathrm{L}}/R_0 = 3.5$, $\hat{\Omega}_{\mathrm{i0}} = 1$). In the first two graphs, red lines show the direction of the magnetic field ($\boldsymbol{B}_{\mathrm{a}}$ and $\tilde{\boldsymbol{B}}_{\mathrm{p}}$ oppose each other at the axis). The normalization factors used in the figures remove the dominant dependencies of each plotted variable.

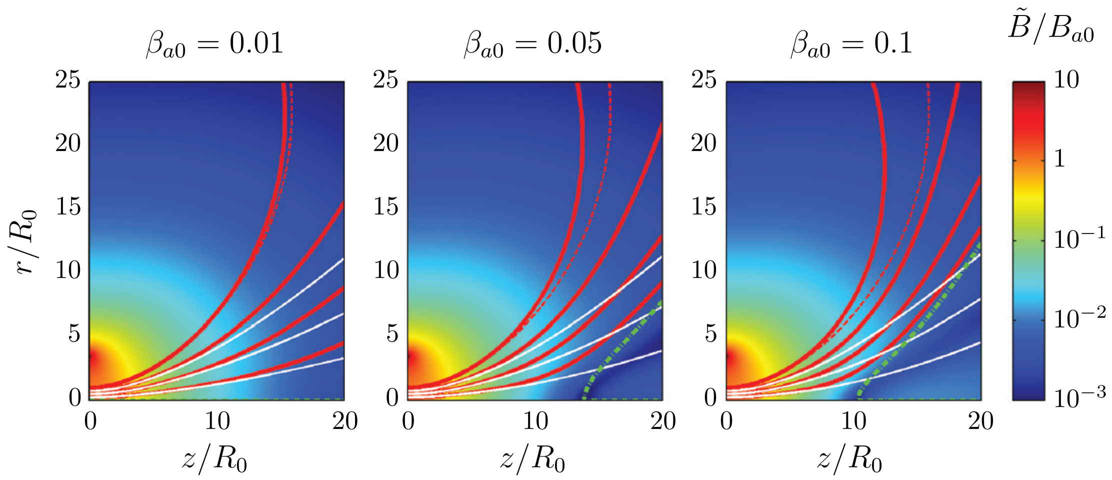

Figure 3. Total longitudinal magnetic field $\tilde{\boldsymbol{B}} = \boldsymbol{B}_{\mathrm{a}} + \tilde{\boldsymbol{B}}_{\mathrm{p}}$ in the MN for $\beta_{\mathrm{a0}} = 0.01$, 0.05 and 0.1 ($\gamma = 1$, $\hat{\Omega}_{\mathrm{i0}} = 1$, $R_{\mathrm{L}}/R_0 = 3.5$). The plasma border and other magnetic streamtubes are indicated as thick red lines. Initially-coincident ion streamtubes are drawn as white, thin lines. For the purpose of comparison, the plasma border for the $\beta_{\mathrm{a0}} = 0$ case is shown as a dashed red line. The existence of a magnetic separatrix is depicted as a dash–dot green line in the last two simulations.

in figure 3, and is marked by the appearance of a point at the axis where $B = 0$, which has also been recovered experimentally [38]. In the region beyond this point, delimited by a separatrix surface (green dash–dot line), the direction of the magnetic field is reversed, and becomes induced-field dominated. This separatrix can therefore be regarded as an 'effective' end boundary to the MN. Since $\tilde{\boldsymbol{B}}_{\mathrm{p}}$ does not substantially affect the strength of the peripheral plasma, the separatrix does not reach the plume edge within the simulated domain, but bends downstream.

In relation to this, the weaker magnetic field boosts plasma demagnetization, especially at the core of the jet. Demagnetization of each species has a fundamentally different effect in the expansion: on the one hand, for the supersonic,

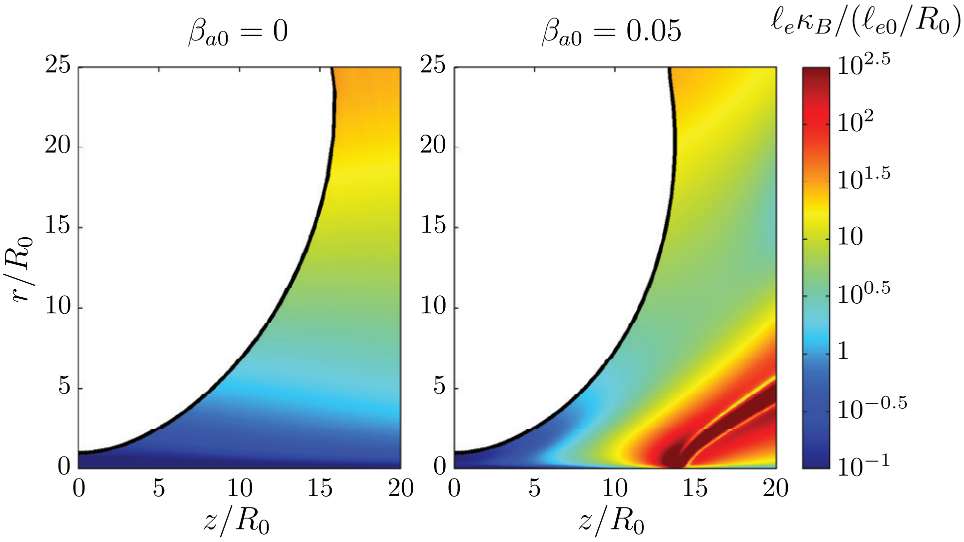

Figure 4. Normalized electron Larmor radius, $\ell_e = \sqrt{m_e T_e}/(eB)$, relative to the local magnetic length, $1/\kappa_B$, for $\beta_{a0} = 0$ and 0.05. The graphs are normalized with the electron Larmor radius at the origin, ℓ_{e0} to make them more general. Typical values of ℓ_{e0}/R_0 in propulsive applications are within 10^{-2}–10^{-3} [6].

mass-carrying ions it is a central mechanism for plasma detachment [18], as it allows the ions to separate inward from the magnetic tubes. This *self-demagnetization* of the central, densest plasma therefore contributes to this detachment process and promotes the formation of a free-expanding plume, as ions are allowed to separate sooner from the magnetic lines.

On the other hand, premature demagnetization of the electrons can lead to increased plume divergence, as the beneficial magnetic force on electrons vanishes and electron confinement is tasked solely to the ambipolar electric field, which expands ions radially. If electron demagnetization occurs too soon (i.e. before ion acceleration is nearly complete and ions are highly hypersonic), this will result in a penalty on the propulsive performance of the MN. This is important specially where electron pressure gradients and therefore the need of magnetic confinement are large (i.e., typically near the plasma edge). The magnetization degree of electrons is measured by the ratio of their local Larmor radius, ℓ_e, to the characteristic macroscopic magnitude of the problem. This can be taken to be the most critical one between R_0 and the local magnetic meridional curvature radius $1/\kappa_B$, with κ_B the meridional magnetic field curvature. This quantity is plotted in figure 4 for $\beta_{a0} = 0$ and 0.05 for comparison. As it can be seen, $\ell_e \kappa_B$ can easily increase about 3 or more orders of magnitude downstream when $\boldsymbol{B}_p$ dominates (particularly if $B \simeq 0$ is reached). Fortunately, in the central part of the jet the electron pressure gradients are low, so this does not impose a heavy penalty on the performance of the MN. On the other hand, the sustained (higher) magnetic field at the peripheral plasma enables the MN to continue to confine the electron pressure in this region which can be regarded as a beneficial effect.

The effect of the enhanced MN divergence caused by $\tilde{\boldsymbol{B}}_p$ on the propulsive performance of the device can be observed in figure 5 with the plume efficiency function, $\eta_{plume}(z)$, defined in [6] as the ratio of axial to total ion kinetic power at a section $z =$ const. Increasing β_{a0} decreases the efficiency, due to the larger radial

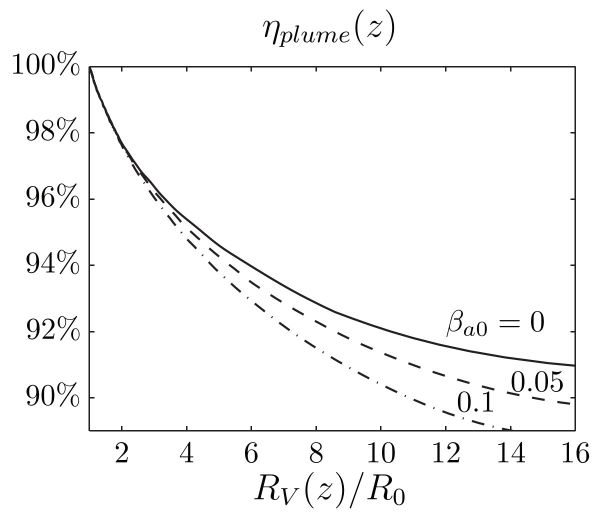

Figure 5. Evolution of the plume divergence efficiency $\eta_{plume}(z)$, for the simulations cases of figure 3. The solid line has $\beta_{a0} = 0.01$, and is visually indistinguishable from the $\beta_{a0} = 0$ case. The dashed line has $\beta_{a0} = 0.05$, and the dash–dot line has $\beta_{a0} = 0.1$.

plasma losses and plume divergence angle. Nonetheless, the effect is visibly small within the β_{a0} range of the present simulations; the reason for this lies in the already advanced state of ion detachment at the section where the changes in MN geometry become important. This is evidenced by the large separation of ion streamtubes with respect to magnetic streamtubes around $z/R_0 = 10$ to 15 in figure 3. Indeed, the divergence angle of the inner ion streamtubes is almost unaffected by the induced magnetic field, and the influence of the larger MN aperture is essentially limited to the low density peripheral plasma.

While the increased plume divergence decreases η_{plume}, the net effect over the thrust function $F(z)/F_0$, i.e. the impulse carried by the jet at a given section z, is smaller than a 1% for the analyzed range of β_{a0} (not shown). It should be kept in mind that the magnetic forces on the plasma due to the magnetic field induced by the plasma currents only, $j_\theta \tilde{B}_p$ and $\tilde{j}\, B_{\theta p}$, are purely internal to the plasma, and therefore cannot contribute directly to thrust; these forces can only cause a redistribution of the plasma properties within the plasma domain.

We now turn our attention to the analysis of the azimuthal induced field, $B_{\theta p}$, generated by the longitudinal electric currents. For a plasma satisfying $j_z = 0$ at the throat, j_z develops downstream as the ion streamtubes separate. Therefore $B_{\theta p}$ is detachment-dependent, and a higher value of $\hat{\Omega}_{i0}$ reduces the magnitude of j_z everywhere [6]. While $j_z \to 0$ downstream due to the geometric expansion, $j_z/(enu_{zi})$ does not vanish in the region of validity of the model.

As ions separate inwards, $j_z > 0$ near the axis, while $j_z < 0$ near the jet boundary in order to satisfy *global* current ambipolarity. As long as this condition is satisfied (as in propulsive applications, where the net charge emitted by a thruster is zero in the steady-state), the integral $\int 2\pi r j_z \mathrm{d}r$ vanishes at every $z = \mathrm{const}$ section. Therefore, $B_{\theta p} = 0$ both at the axis and at the plasma edge: i.e. there is no induction of $B_{\theta p}$ outside of the plasma domain.

According to equation (10), $B_{\theta p} > 0$ within the plasma volume. The sign of $\tilde{j} B_{\theta p}$ is inverted when the $j_z = 0$ condition is placed at a section downstream, e.g. in the presence of a dielectric target for material processing with MNs (see figure 8 of [6]). Notwithstanding this, observe that the magnetic force $\tilde{j} B_{\theta p}$ always acts in the outward direction in the plasma periphery, and therefore tends to increase plume divergence.

Figure 6 displays j_z and $B_{\theta p}$ for the simulation with $\beta_{a0} = 0.01$. A first observation is that while j_z becomes comparable to the ion current downstream, its absolute value is nonetheless small, and $B_{\theta p}$ is negligible in all cases of interest. Therefore, the azimuthal induced field is only a secondary feature of the near region expansion, compared to the longitudinal $\tilde{B}_p$. While the breakdown of isorotation described before (equation (4)) means a small change in $u_{\theta e}$ and the Hall force density on the electrons, $j_{\theta e} \tilde{B} \mathbf{1}_\perp$, the electron balance of forces is essentially unaffected by the presence of $B_{\theta p}$. Nonetheless, it couples the calculation of $u_{\theta e}$ with $u_{\parallel e}$, and it could lead to a large value of $u_{\theta e}$ especially in the neighborhood of a $B = 0$ point, if present.

To close this section, it is noted that our plasma/MN model presents the following limitations related to the calculation of the induced field effects. First, the calculation of electron properties in the fully-magnetized electron model is based on the propagation of the $H_e(\psi)$ function along magnetic lines ($\psi = \mathrm{const}$). This function is defined at the MN throat from $\psi = 0$ (the axis) to $\psi = \psi_V$, the value at the plasma-vacuum edge. However, after the separatrix it is $\psi < 0$ and H_e is undefined. In the absence of a better criterion, we have opted here to maintain $H_e(\psi < 0) = H_e(0)$, under the assumption that the electrons that fill the region beyond the separatrix have a similar value of this integration constant to that of electrons at the axis. This, in particular, leads to $j_{\theta e} = 0$ in this region. The error committed by this assumption is expected to be small within the simulated domain. Indeed, the fully-magnetized electron condition breaks down when the magnetic strength approaches zero. As the magnetic field diminishes, additional phenomena (resistivity, electron inertia, the gyroviscous force [35, 39]) may gain relevance in the electron equation of motion, which are neglected in the present model. These effects can initiate electron separation from the magnetic tubes and change their currents [17].

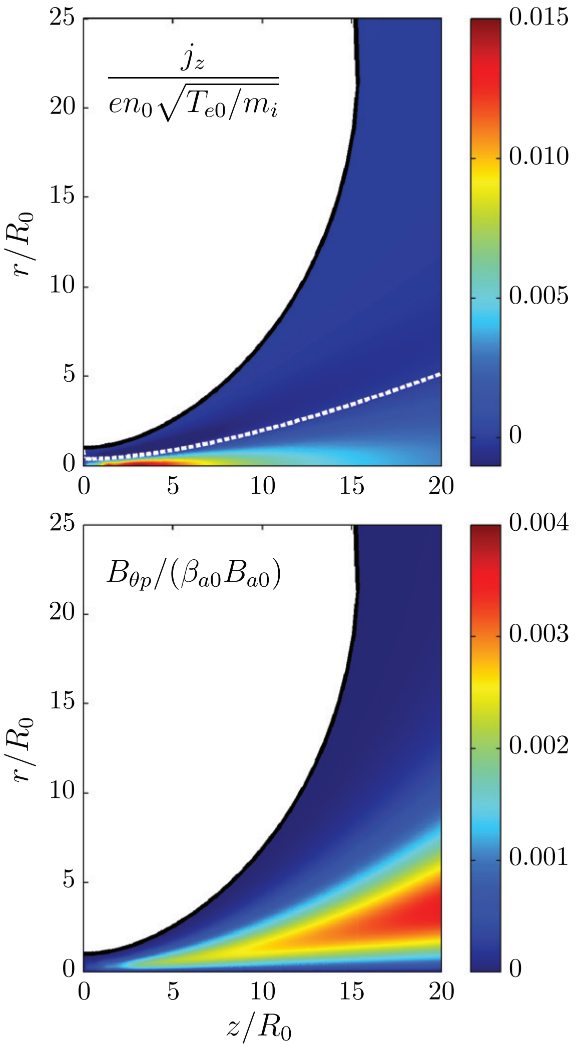

Figure 6. Axial electric current j_z and azimuthal induced magnetic field $B_{\theta p}/B$, in the $\beta_{a0} = 0.01$ case. The white dashed line in the first plot indicates the location where $j_z = 0$.

Consequently, the present model cannot provide a faithful description of the azimuthal currents when $B \to 0$, where a partially-magnetized electron model is needed. This affects, in particular, the region near the predicted separatrix. While the cancellation of the magnetic field at the axis (and the formation of a separatrix) depends primarily on the azimuthal electric currents that exist up to that point, a partially-magnetized electron model is needed to confirm the presence of this feature of the magnetic field, its actual shape, and the subsequent evolution of the plasma downstream of it. Such model will also enable the closure of the longitudinal electric currents downstream.

Lastly, our gross Maxwellian, isotropic, isothermal electron model neglects the evolution of the electron velocity distribution function in the nozzle, which is affected by the set up of potential barriers [32]. While these aspects are important to obtain an accurate electron model, they are not expected to interfere with the central conclusions of the present work, which merely rely on the diamagnetic nature of the plasma expanding in the divergent field.

5. Conclusion

The two-fluid model of the plasma expansion in a divergent magnetic nozzle of [6] has been extended to include the plasma-induced magnetic field and assess its effect on the expansion and the MN shape. An analytical study in the paraxial limit has been undertaken, followed by the full 2D numerical integration of the model to confirm and extend the conclusions of the 1D approximation. The induced field effects have been characterized as a function of β_{a0}, the main parameter in the discussion. The effect on $\boldsymbol{B}_p$ of an effective electron cooling rate, γ, has also been commented on. While the focus of the article are propulsive MNs in space plasma thrusters, its conclusions are easily extrapolable to similar devices and configurations in plasma manufacturing, material processing and supersonic plasma wind tunnels.

It has been shown that the plasma-induced magnetic field, inherently diamagnetic in a warm sonic plasma expanding in a mild magnetic field, increases the aperture of the nozzle, resulting in a more divergent jet. At the same time, the induced field weakens the magnetic strength in the central part of the MN, and enhances the demagnetization of the core beam. The larger divergence deteriorates slightly the propulsive performance of the MN as measured by $\eta_{\text{plume}}(z)$. Paramagnetic expansions, such as those of an initially-hypersonic (i.e. cold) plasma or extremely high ion magnetization levels [17] are not of propulsive interest and have not been covered in this work.

A faster electron cooling rate (i.e. higher γ) reduces the magnitude of these effects. The induced magnetic field is markedly 2D, and concentrates in the region around the MN axis, while in the periphery of the plasma the magnetic field strength remains essentially constant. Already at rather small values of β_{a0}, the longitudinal induced field can cancel out the magnetic field at the axis of the jet, as observed experimentally [38], reversing its direction and forming a separatrix surface that marks the transition to an induced-field dominated region. Confirming the presence of such feature (and studying the downstream evolution of the plasma) requires an unmagnetized electron model, which is beyond the scope of the present work. The azimuthal induced field, on the other hand, is essentially negligible in most applications, but modifies the azimuthal electron current where the longitudinal field is low. This effect decreases with increasing $\hat{\Omega}_{i0}$.

Acknowledgments

The authors would like to thank M Martínez-Sánchez for the insightful discussions. Initial work was sponsored by the Air Force Office of Scientific Research, Air Force Material Command, USAF (FA8655-12-1-2043). Additional support was provided by Spanish R&D National Plan (grant number ESP2013-41052-P). Preliminary versions of this work were presented in a conference [37].

References

[1] Andersen S, Jensen V, Nielsen P and D'Angelo N 1969 *Phys. Fluids* **12** 557–60
[2] Kuriki K and Okada O 1970 *Phys. Fluids* **13** 2262
[3] York T M, Jacoby B A and Mikellides P 1992 *J. Propulsion Power* **8** 1023–30
[4] Inutake M, Ando A, Hattori K, Tobari H and Yagai T 2002 *J. Plasma Fusion Res.* **78** 1352–60
[5] Takama Y and Suzuki K 2008 *Plasma Sources Sci. Technol.* **17** 015005
[6] Ahedo E and Merino M 2010 *Phys. Plasmas* **17** 073501
[7] Krülle G, Auweter-Kurtz M and Sasoh A 1998 *J. Propulsion Power* **14** 754–63
[8] Arefiev A and Breizman B 2004 *Phys. Plasmas* **11** 2942–9
[9] Charles C and Boswell R 2003 *Appl. Phys. Lett.* **82** 1356
[10] Prager J, Winglee R, Ziemba T, Roberson B and Quetin G 2008 *Plasma Sources Sci. Technol.* **17** 025003
[11] Batishchev O 2009 *IEEE Trans. Plasma Sci.* **37** 1563–71
[12] Pottinger S, Lappas V, Charles C and Boswell R 2011 *J. Phys. D: Appl. Phys.* **44** 235201
[13] Ahedo E 2011 *Plasma Phys. Control. Fusion* **53** 124037
[14] Williams L T and Walker M L 2013 *J. Propulsion Power* **29** 520–7
[15] Shabshelowitz A and Gallimore A 2013 *J. Propulsion Power* **29** 919–29
[16] Gerwin R, Marklin G, Sgro A and Glasser A 1990 Characterization of plasma flow through magnetic nozzles *Technical Report* AFSOR AL-TR-89-092, Los Alamos National Laboratory
[17] Ahedo E and Merino M 2011 *Phys. Plasmas* **18** 053504
[18] Merino M and Ahedo E 2014 *Plasma Sources Sci. Technol.* **23** 032001
[19] Hoyt R, Scheuer J, Schoenberg K, Gerwin R, Moses R and Henins I 1995 *IEEE Trans. Plasma Sci.* **23** 481–94
[20] Schoenberg K, Gerwin R, Moses R, Scheuer J and Wagner H 1998 *Phys. Plasmas* **5** 2090–104
[21] Longmier B *et al* 2011 *Plasma Sources Sci. Technol.* **20** 015007
[22] Arefiev A and Breizman B 2005 *Phys. Plasmas* **12** 043504
[23] Winglee R, Ziemba T, Giersch L, Prager J, Carscadden J and Roberson B 2007 *Phys. Plasmas* **14** 063501
[24] Ahedo E 2009 *Phys. Plasmas* **16** 113503
[25] Ahedo E 2011 *Phys. Plasmas* **18** 103506
[26] Gerwin R A 2009 Integrity of the plasma magnetic nozzle *Technical Report* NASA/TP-2009-213439
[27] Takahashi K, Lafleur T, Charles C, Alexander P and Boswell R 2011 *Phys. Rev. Lett.* **107** 235001
[28] Merino M and Ahedo E 2013 *Phys. Plasmas* **20** 023502
[29] Merino M and Ahedo E 2015 *IEEE Trans. Plasma Sci.* **43** 244–51
[30] Deline C, Bengtson R, Breizman B, Tushentsov M, Jones J, Chavers D, Dobson C and Schuettpelz B 2009 *Phys. Plasmas* **16** 033502
[31] Sheehan J P *et al* 2014 *Plasma Sources Sci. Technol.* **23** 045014
[32] Martinez-Sanchez M, Navarro-Cavallé J and Ahedo E 2015 *Phys. Plasmas* **22** 053501
[33] Hu Y and Wang J 2015 *IEEE Trans. Plasma Sci.* **43** 2832–8
[34] Chandrasekhar S 1956 *Astrophys. J.* **124** 232
[35] Ahedo E and Merino M 2012 *Phys. Plasmas* **19** 083501
[36] Merino M and Ahedo E 2016 *Phys. Plasmas* **23** 023506
[37] Merino M and Ahedo E 2011 Plasma detachment mechanisms in a magnetic nozzle *47th AIAA/ASME/SAE/ASEE Joint Propulsion Conference & Exhibit* (Washington, DC: AIAA) AIAA-2011-5999
[38] Roberson B, Winglee R and Prager J 2011 *Phys. Plasmas* **18** 053505
[39] Ramos J 2005 *Phys. Plasmas* **12** 112301